▌ **Supramolecular Nanostructures**

Supramolecular Nanoassemblies of an Amphiphilic Porphyrin–Cyclodextrin Conjugate and Their Morphological Transition from Vesicle to Network

Jin Zhao, Heng-Yi Zhang, He-Lue Sun, and Yu Liu*[a]

Abstract: An amphiphilic compound, 5-(4′-dodecyloxy-phenyl)-10,15,20-tri(permethyl-β-CD)-modified Zn^{II}–porphyrin (**1**; β-CD = β-cyclodextrin), was synthesized by means of the click reaction of an alkylated Zn–porphyrin derivative with 6-deoxy-6-azidopermethyl-β-CD. The complexation between **1** and tetrasodium tetraphenylporphyrintetrasulfonate (**5**) with different molar ratios led to the formation of two distinctly different nanoarchitectures, which were proven to be vesicle and network aggregates, respectively, by using dynamic light scattering, scanning electron microscopy, transmission electron microscopy, and atomic force microscopy. On the basis of the results of the time-dependent TEM studies, fluorescence, and NMR spectroscopic measurements, we have determined that the mechanism of the morphology transition from vesicles to networks is controlled by the stepwise complexation of **1** with **5**. Furthermore, these supramolecular nanoarchitectures show the controlled-release property of doxorubicin as potential candidates for drug delivery.

Introduction

The controlled construction of nanoscale soft materials with desired nanostructures offers great potential applications in various fields.[1] Since nanomaterials formed from the same or similar components with different morphologies can have distinctly different physicochemical properties, the precise control of their shapes, sizes, and dimensions are especially important.[2] Self-assembly is considered a promising approach for controlled realization of materials with well-defined nanostructures owing to the facile synthesis and the reversible property.[3] However, it is very difficult to change the parameters that determine the behaviors and interactions of supramolecular system components in the process of self-assembly.[4] Thus, one challenge would be to design molecular building blocks in which these parameters could be changed easily for organizing themselves into desired patterns and functions. Among self-assembly architectures, vesicles represent an important class of materials with special roles in the fields of drug delivery, microreactors, filters, and artificial biomembranes.[5] At the same time, nanofibers and nanonetworks have attracted increasing attention because of their versatile properties, which result in potential applications in optoelectronic devices, chemical sensor, and catalysis, and so on.[6] Up to now, there have

been few reports on the morphological transition between vesicles and nanofibers.[7] For instance, Yao and Zhan et al. reported a reversible transition between nanofibers and vesicles by using external stimuli of temperature and ultrasound.[7a] Moreover, Ghosh and co-workers constructed a vesicular assembly from a naphthalene-diimide-based bolaamphiphile, which can transit into fibers by means of intercalation of an electron-rich pyrene.[7d]

However, porphyrins have been widely used as functional components in supramolecular chemistry owing to their unique photochemical and electroactive properties.[8] In particular, the integration of porphyrin and cyclodextrin (CD) becomes an important topic for constructing functional supramolecular assemblies.[9] Considerable efforts have been made to prepare porphyrin–CD conjugates for the development of artificial photosynthetic systems, delivery systems in therapy and diagnosis, dioxygen transport protein mimetic systems, and so on.[10] Breslow and co-workers modeled cytochrome P-450 by utilizing porphyrin–β-CD conjugates, in which the opposing CD units were able to cooperatively bind the substrates and the porphyrin could be used as catalysts for substrate oxidation.[10h,i] In our previous work, we presented the morphological transition of nanorods to network aggregates constructed from structurally similar porphyrin–CD conjugates, which was controlled by the complexation strength of porphyrins with CDs.[9a] Herein, we will report that a porphyrin–permethyl-β-CD conjugate **1**, which bears a dodecyl side chain on one side of the porphyrin core, self-assembles into nanoscale vesicles and fibers in aqueous solution, respectively. The transition from vesicles to nanofiber aggregates is controlled by the stepwise complexation of compound **1** with tetrasodium tetraphenyl-porphyrintetrasulfonate (**5**) by changing the host/guest stoichi-

[a] J. Zhao, Prof. Dr. H.-Y. Zhang, H.-L. Sun, Prof. Dr. Y. Liu
Department of Chemistry
State Key Laboratory of Elemento-Organic Chemistry, Nankai University
Collaborative Innovation Center of Chemical Science and Engineering
Tianjin 300071 (China)
E-mail: yuliu@nankai.edu.cn

🖳 Supporting information for this article is available on the WWW under
http://dx.doi.org/10.1002/chem.201405943.

ometry ratio. Both vesicles and networks can be applied as potential drug carriers. The release rate of doxorubicin hydrochloride (DOX) is distinctly different in these drug-encapsulated supramolecular assemblies. Thus, the release rate of loaded agents can be satisfactorily controlled by changing the host/guest molar ratio.
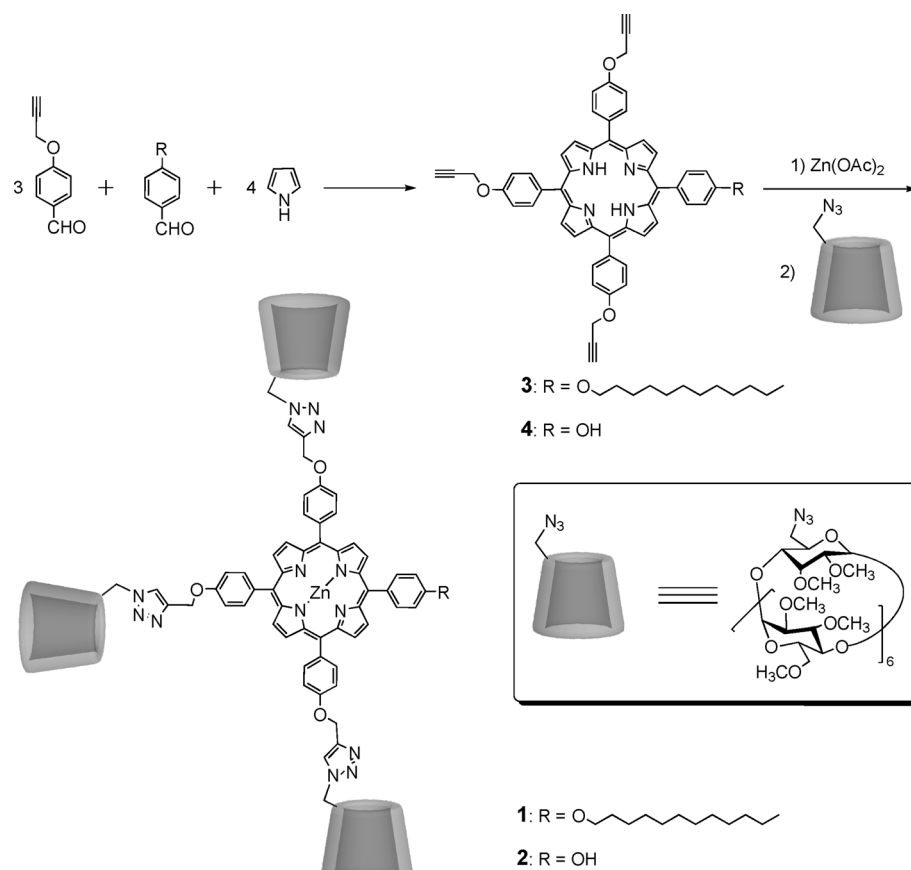
Results and Discussion

Synthesis

The reactions of benzaldehyde derivatives with pyrrole in propionic acid afforded the porphyrin derivatives **3** (6% yield) and **4** (5% yield), respectively. After being coordinated with Zn^{2+}, the two resulting Zn–porphyrin derivatives further reacted with 6-deoxy-6-azidopermethyl-β-CD to obtain compounds **1** (90% yield) and **2** (70% yield), respectively, by means of "click chemistry" (Scheme 1), from which the supramolecular nanoarchitectures were constructed by the complexation of **5** with **2** and **1** in aqueous solution.[11]

Scheme 1. Synthetic routes to compounds **1** and **2**.

Dynamic light scattering (DLS) and microscopy analyses

DLS was used to determine the hydrodynamic diameter (D_H) of the aggregate of **1** and **5** with different stoichiometries in aqueous solution. In the case of a 1:0.5 stoichiometric ratio for **1** and **5**, the D_H value of the resultant aggregate is centered at about 204 nm. Surprisingly, the corresponding D_H value increases to 546 nm when the stoichiometry is changed to 1:1.5 (Figure S33 in the Supporting Information). These size-distribution differences clearly indicate that different supramolecular aggregates exist in the presence of **5**.

To identify the morphologies of the supramolecular aggregates in different stoichiometric ratios, we first performed scanning electron microscopy (SEM), atomic force microscopy (AFM), and transmission electron microscopy (TEM) experiments in 1:0.5 stoichiometry of **1** with **5**.

As can be seen from Figure 1a, only spherical objects with an approximately 200 nm diameter can be observed in the SEM image. Similarly, such spheres are also observed in the AFM image (Figure 1b), in which the vertical distances of the spheres are approximately 20 nm and the horizontal distances are about 225 nm. That is, the height-to-diameter ratio of the dried spherical particles is up to 1:11, which suggests a collapsed vesicular structure.[12] Its TEM image shows a number of
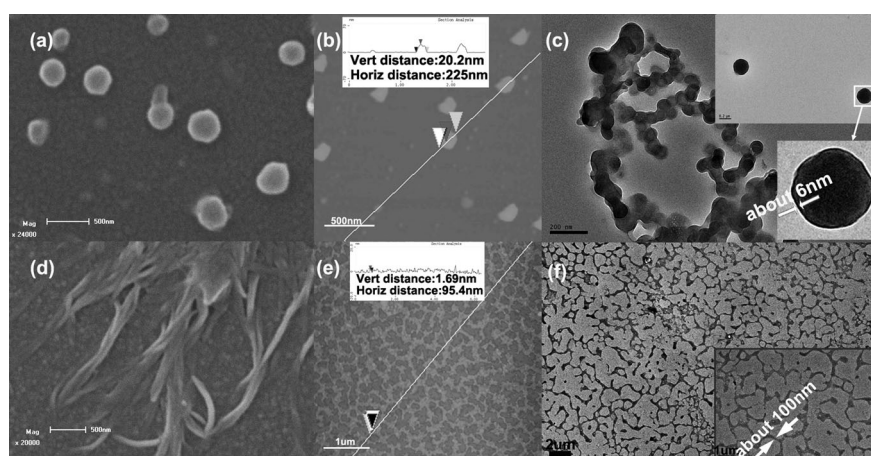

Figure 1. a, d) SEM, b, e) AFM, and c, f) TEM images of the supramolecular aggregates formed by the complexation of **1** with **5** in a–c) 1:0.5 and in d–f) 1:1.5 molar ratio, respectively.

spheres with diameters in the range of 100–230 nm (Figure 1c). The contrast of periphery and central parts is distinguishable, thus indicating that the morphology of the aggregates should be a hollow vesicular structure. On the basis of a statistical analysis of 20 vesicles in the TEM image, we calculated that the thickness of the membrane is about 6–8 nm, which fits approximately with a bilayer estimated by 3D molecular structural modeling of complex 1·5 in a 1:0.5 molar ratio (Figure S23 in the Supporting Information). Therefore, we deduced that the vesicles should adopt a binary structure, in which the inner and outer hydrophilic shell layers are composed of the highly stable CD/5-associated units with porphyrin spacers, whereas the hydrophobic aliphatic chains interlace with each other in the middle of the vesicles (Figure 2).

In sharp contrast, the aggregates formed by the complexation of 1 with 5 in a 1:1.5 molar ratio are distinctly different from those in a 1:0.5 ratio in their morphologies. Both the SEM and the AFM images show fiberlike aggregates. The entwined nanofibers with widths that range from 50 to 150 nm are observed in the SEM image, and the sizes in the AFM image have widths of 60–110 nm and heights of approximately 1.7 nm. Considering the calculated length of the aliphatic chains in the oligomers is about 11 nm (Figure S24 in the Supporting Information), one could reasonably deduce that the aliphatic chains should adopt a parallel arrangement on the mica surface. On the basis of the above deduction, we could estimate that the aggregates should be formed from the bundling of about 50 polymer chains by entangling the aliphatic chains through van der Waals interactions.[8d,e,13] The linear polymers would further aggregate into nanonetwork assemblies due to the interaction between aliphatic chains and the deficient complexation of 1 with 5 (Figure S25 in the Supporting Information). The TEM image also shows the networklike structures, which is similar to the observations in SEM and AFM images.

The formation of these two distinct nanoarchitectures led us to investigate the origin of the difference, and we proceeded to record the TEM images of the assembly in a 1:1.5 stoichiometric ratio at different time intervals. Several individual vesicular aggregates with diameters of approximately 200 nm were observed from the freshly prepared sample (Figure 2). After 6 h, some 1D fibers attached on the surface of the vesicular assembly, and then these vesicular aggregates disappeared completely to become 1D fibers after approximately 12 h. Eventually, these 1D fibers were found in the form of a cross-linked network after 32 h. On the basis of the aforementioned morphological variation, we propose that the mechanism of morphological transition from vesicles to network fiber aggregates is as follows. When 1 equivalent of compound 1 was freshly mixed with 1.5 equivalents of 5, 1 equivalent of 1 interacted previously with only 0.5 equivalents of 5 to form vesicular aggregates owing to its amphiphilic property. Subsequently, the excess amount of guest 5 embedded in the membranes of vesicles, which was supported by the ζ-potential measurements.[14] Then the self-included CD units were extracted and encapsulated the embedded 5 to produce 1D fibers because of the strong binding ability between permethylated-β-CD and 5. These nanofibers could exist in the form of a network owing to the bundling of fibers by the entanglement of the aliphatic chains and deficient complexation (Figure S25 in the Supporting Information).[15] Moreover, time-dependent DLS was also performed to further support the proposed transition mechanism from vesicle to network. Upon the addition of an excess amount of 5 into the vesicular solution, both the hydrodynamic diameter (D_H) and the polydispersity of the assembly increased. After 12 h, a hydrodynamic diameter centered at 51.79 μm could be observed, thus indicating that a larger assembly was formed (Figures S38 and S39 in the Supporting Information). In addition, the specific conductance change of the vesicular solution after the addition of an excess amount of 5 was measured. The increasing specific conductance is mainly attributed to the formation of the interconnected 3D network assembly. The specific conductance changes can also further support the morphological transition of the assemblies.
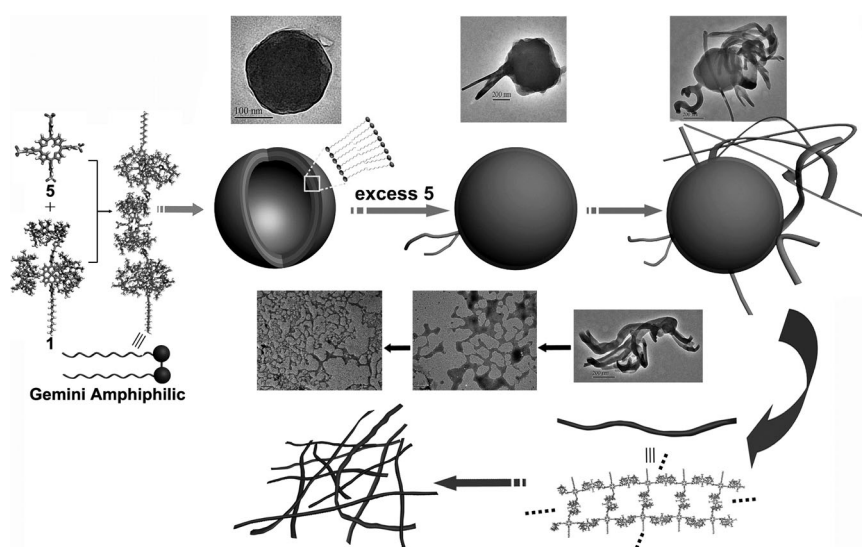
Fluorescence measurements

To further support the mechanism of the morphology transition described above, fluorescence spectroscopy experiments were carried out. The solubility of 1 in water is limited, but the addition of 5 improves dramatically its solubility. This observation suggests that complexation exists between 1 and 5.[9a,11f] The quantitative investigation of the host–guest interaction was examined by means of fluorescence titration. As can be seen from Figure 3, upon addition of 5 into a solution of 1, the
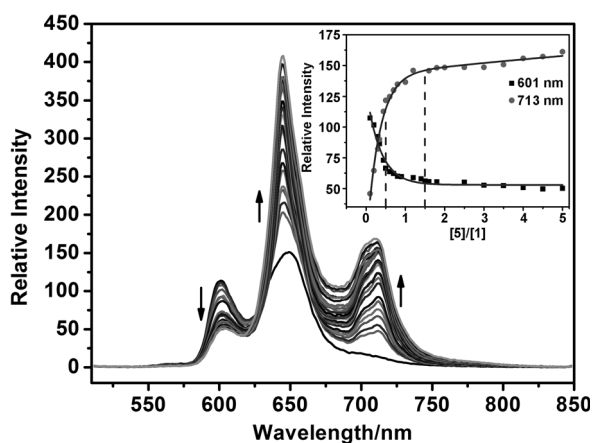

Figure 2. Schematic representation of the guest-induced morphological transition from vesicle to network.

Figure 3. Emission spectra of **1** (1.0×10^{-6} M) upon addition of **5** in phosphate buffer solution (pH 7.2, $\lambda_{ex} = 432$ nm). Inset: Fluorescence intensity changes versus the molar ratio of **5**/**1** recorded at $\lambda = 601$ and 713 nm, respectively.

fluorescence intensity of **1** at 601 nm decreased, whereas that at 713 nm increased. The fluorescence change could be attributed to the complexation and slight energy-transfer process. Moreover, we also investigated the complexation stoichiometry between **1** and **5** by means of fluorescence spectrometry. The curve of the fluorescence intensity versus the [**5**]/[**1**] molar ratio shows two inflection points at molar ratios of 0.5 and 1.5, thereby implying that the 1:1.5 stoichiometry complex is formed by stepwise binding of **1** and **5**. The Job plot further confirmed the same stoichiometry (Figure S12 in the Supporting Information).

In addition, pyrene was selected as a probe molecule to estimate the critical aggregation concentration (CAC) of the **1·5** complex in a 1:0.5 stoichiometric ratio by measuring its fluorescence intensity change.[16] The ratio of intensities of the first and third vibronic peaks of pyrene (I_1/I_3) is intimately associated with the polarity of its solubilization environment. The fluorescence spectra that contain pyrene probe molecules show that the fluorescence intensity of pyrene diminishes with increasing complex concentration. The curve of the fluorescence intensity ratio versus the concentration shows an inflexion point at 8×10^{-7} M, thus indicating the formation of the vesicle assemblies above this concentration. From this result, the CAC is estimated to be 8×10^{-7} M, which is in good agreement with the result from the DLS measurements by plotting the scattering intensity versus the complex concentration. The results of DLS show that the scattering intensity increased with increasing complex concentration, but the size of aggregation barely changes (Figures S26 and S27 in the Supporting Information).

NMR spectra

We further investigated the complexation process of **1** with **5** by means of NMR spectroscopy. Owing to the low solubility of **1** in aqueous solution, a similar structural compound **2** was chosen as a model molecule to investigate the host–guest complexation process. Firstly, the conformation of host **2** in both water and organic solvents was determined. As shown in
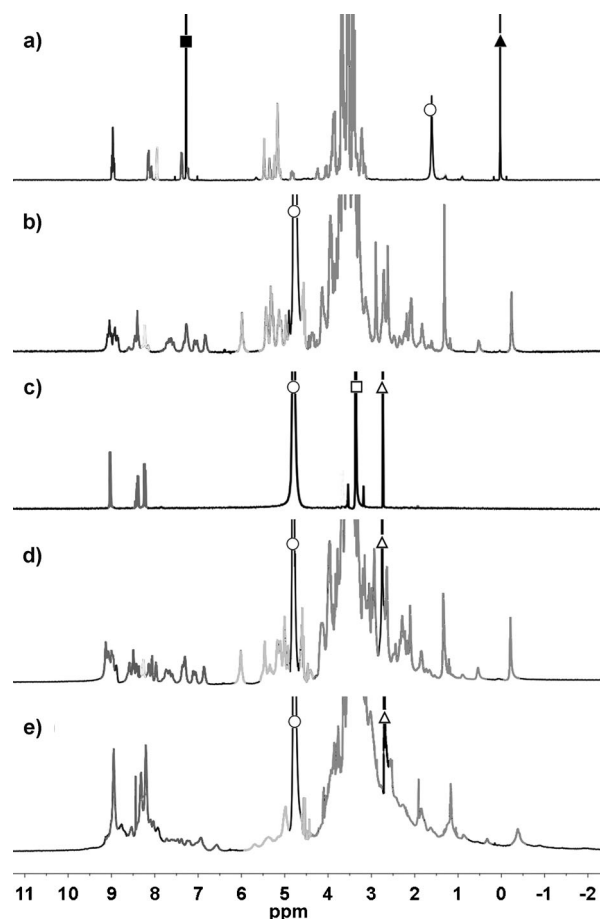

Figure 4. ^{1}H NMR spectra of a) **2** in CDCl$_3$, b) **2** in D$_2$O, c) **5** in D$_2$O, d) **2** with **5** in a 1:0.5 molar ratio in D$_2$O, and e) **2** with **5** in a 1:1.5 molar ratio in D$_2$O. Symbols: ■, ○, and ▲ represent residual solvent, H$_2$O, and tetramethylsilane (TMS) in CDCl$_3$. Symbols ○, □, and △ indicate residual solvent HOD, MeOH, and DMSO resonances, respectively, and MeOH was chosen as reference in D$_2$O.

Figure 4, the ^{1}H NMR spectrum of **2** in CDCl$_3$ is distinctly different from that in D$_2$O. In CDCl$_3$, the peaks at $\delta = 8.95$, 8.13, 8.07, 7.94, 7.36, and 7.22 ppm are assigned to the protons of the pyrrole, the *ortho*-phenyl moieties, the triazole rings, and the *meta*-phenyl moieties, respectively, which was confirmed by the 2D COSY spectrum (Figure S9 in the Supporting Information). Interestingly, compound **2** in D$_2$O exhibits a sharply different spectrum to that in CDCl$_3$. The peaks assigned to the pyrrole rings and aromatic rings of **2** are broadened and split into several different subsets that accompany the variation in chemical shifts. In addition, there are some new peaks in the range of $\delta = -0.5$–2.0 ppm in D$_2$O, which are not observed below $\delta = 3.0$ ppm in CDCl$_3$. These signals are attributed to the protons of the OCH$_3$ groups on the second main of the CD moieties according to the previous reported results.[9a] This attribution is also supported by the heteronuclear single quantum correlation (HSQC) spectrum of **2** in D$_2$O (Figure S14 in the Supporting Information). Additional insight into the conformation of **2** is gained by means of a 2D NOESY spectrum in D$_2$O (Figure S16 in the Supporting Information). It is shown that there are strong cross-peaks between the aromatic pro-

tons and the inner protons of the CD unit. At the same time, weak cross-peaks of the pyrrole and phenyl protons with a CD secondary-face methoxy group are also detected. These observations suggest that the conformation of **2** is a deep inclusion of the phenyl group in the CD cavity in aqueous solution.

On the basis of previous reports,[9a, 17] the self-included conformation is formed by undergoing a 360° rotation of the substituted glucopyranose unit around the α-1,4-glycosidic bonds. In addition, we speculated that only in the opposite positions did two permethylated CD units of **2** intramolecularly include the porphyrin spacer owing to steric hindrance of CD units around the porphyrin core. This conformation of **2** was also validated by the molecular-mechanics results with a Dreiding force field (Figure S18 in the Supporting Information). Conversely, the conformation of **2** was an expansive mode in chloroform.

Although the solubility of compound **1** in water is very limited, a slight clear ^{1}H NMR spectrum of **1** could be obtained in D_2O/CD_3OD (v/v 9:1) solution (Figure S17 in the Supporting Information). Similarly, the signals in the low field show a clear broadening, splitting, and shifting, whereas those new peaks below $\delta = 3.0$ ppm are also detected relative to **1** in CDCl$_3$. On the basis of the above observations, we deduced that, like **2**, compound **1** also exists in the self-included conformation in aqueous solution.

There are four phenyl sulfonic groups in **5**, and the opposing pairs of them can interact with the cavities of CD.[9a, 10f,g] Upon the addition of **5** into an aqueous solution of **1**,[18] this compound is first likely to form an intermolecular inclusion complex of **1** in a 1:0.5 molar ratio. As shown in Figure 2, a Gemini amphiphilic complex forms and self-assembles into organized supramolecular assemblies. When the excess amount of **5** was added into the solution, the two self-included permethylated CD units are extracted from the porphyrin core into the expansive mode because of the strong binding ability between the CD cavities of **1** and the phenylsulfonic groups of **5**.[9a, 11f] As a result, all three permethylated CD cavities can include **5** in a 1:1.5 molar ratio, thus leading to the formation of a different assembly.

To confirm this supposed complexation process, the model molecule **2** was further used to provide evidence about the interaction of permethylated CD and **5** by examining its 2D NOESY spectrum. The clear nuclear Overhauser effect (NOE) correlations between the permethylated CD protons of **2** with the aromatic protons of the pyrrole of the porphyrin as well as the phenyl groups of **2** and **5** have been detected in a 1:0.5 molar ratio in D_2O, thus suggesting the formation of the complex **2·5** although the self-included conformation of **2** is not affected (Figure S21 in the Supporting Information). The coherent explanation of the above observed results was the first binding of **5** with the expansive CD moieties of **2**. In contrast, only the cross-peaks between the aromatic protons of **5** and the CD protons of **2** are observed after adding an excess amount of guest **5** (Figure S22 in the Supporting Information). This phenomenon evidently indicates that the self-included CD moieties recover to the expansive mode by inversion of the substituted glucopyranose unit for further complexation with

5. All these observations show that the binding between the model molecule **2** and guest **5** is a stepwise process. As for **1**, we can conclude that the binding of **1** with **5** adopts the same stepwise complexation. Therefore, different types of complexes were formed and different morphological supramolecular assemblies were fabricated by means of the complexes self-organizing.

With regard to the speculated network packing mode, diffusion-ordered spectroscopy (DOSY) experiments were performed to further support the deduction (Figures S35 and S36 in the Supporting Information). The diffusion coefficients for complex **2·5** in 1:0.5 and 1:1.5 molar ratios are 5.75 and 5.42 × 10^{-11} m^2 s^{-1}, respectively. The former is relatively higher than the latter, thus indicating that the complex **2·5** in a 1:1.5 molar ratio would exist in the larger fiber form. Moreover, in the logarithmic plot of the specific viscosity versus the concentration of **1·5** and **2·5** in a 1:1.5 molar ratio, the clear inflection points at 0.75 and 1.5 × 10^{-4} M, respectively, as the CAC are observed (Figure S34 in the Supporting Information). Relative to **2·5**, the lower CAC value for **1·5** is mainly attributed to the van der Waals interaction between the aliphatic chains of **1**. In addition, the specific viscosity value of **1·5** is larger than that of **2·5** for the same concentration above the CAC, which further demonstrates the entangling of the aliphatic chains in a network assembly.

Loading and in vitro release of DOX

Drug delivery and controlled-release systems have attracted more and more attention owing to their benefits such as therapeutic effects, reduced toxicity, decreased medication time, and so on.[19] Herein, we chose doxorubicin hydrochloride (DOX), a kind of fluorescent dye and anticancer drug, as a model drug molecule. We first examined the capability of encapsulation and release of these supramolecular assemblies for DOX. After the assemblies were mixed with DOX, extensive dialysis was carried out to ensure the complete removal of the unloaded DOX. In comparison with the unloaded assemblies, the emission spectrum of the loaded assemblies shows a distinct emission band from 510 to 600 nm that arises from the encapsulated DOX (Figure S29 in the Supporting Information). This observation indicates that the anticancer drug DOX can be loaded into this vesicle container. The confocal fluorescence microscopy image also reveals red-light-emitting spherical particles. In addition, the network aggregations can also easily load DOX through the strong electrostatic interaction between the DOX and the sulfonate groups.

The release behavior of these assemblies with different morphologies was further investigated to verify their ability as drug carriers to load DOX. The drug-release profiles of the supramolecular-assembly-loaded DOX and the corresponding free DOX in ultrapure water are presented in Figure 5. The DOX release profile shows that the rates of DOX release in the solution of DOX-loaded assemblies are slower than that of the free DOX solution. It is worth noting that the release rates of DOX loaded in vesicles and networks are also different. The release rate from the networks assembly is slower than that from
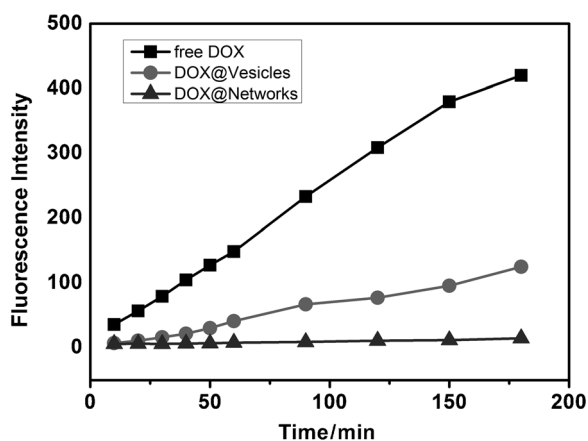
Figure 5. In vitro release profiles of DOX from the DOX@vesicles (●), DOX@networks (▲), and free DOX (■) in aqueous solution.

the vesicles. These results jointly demonstrated that the controlled-release systems with different DOX release rates could be obtained and tuned easily through the **1·5** self-assembly and the morphology transition. Therefore, these supramolecular assemblies can serve as new nanocapsules to load and release drug agents and might find clinical applications.

Conclusion

In summary, we synthesized an amphiphilic porphyrin–permethyl-β-CD conjugate **1** by means of a click reaction in a satisfactory yield and then constructed two distinctly different supramolecular aggregates by the complexation of **1** with **5** in different molar ratios. The time-dependent TEM experiments demonstrated the process of the morphological transition from vesicles to networks, and the NMR spectroscopic results suggested that the origin of the morphological transition is ascribable to the 360° rotation of the opposing pairs of CD units induced by guest **5**. In addition, these supramolecular aggregates can encapsulate drug molecules as nanocontainers for drug delivery and controlled release. The present work not only provides a novel approach to easily construct supramolecular nanoarchitectures with desired nanostructures, but also paves a feasible way to rationally design the drug delivery systems with different controlled-release abilities.

Experimental Section

Materials

Compound **5** was purchased from Acros, and β-cyclodextrin was purchased from Wako. 6-Deoxy-6-azidopermethyl-β-CD was prepared according to the procedure described previously. All other reagents were commercially available and used as received unless stated otherwise. Column chromatography was performed on silica gel (200–300 mesh).

Measurements

NMR spectra were recorded using a Bruker AV400 instrument or a Varian Mercury VX-300 spectrometer in D_2O and $CDCl_3$ by using

tetramethylsilane or MeOH as internal references. Matrix-assisted laser desorption ionization mass spectrometry (MALDI-MS) was measured using a Varian 7.0T FTMS in positive-ion mode. Electrospray ionization mass spectra (ESI-MS) were measured using an Agilent 6520 Q-TOF-MS in positive-ion mode. Elemental analyses were recorded using a Perkin–Elmer 2400C instrument.

UV/Vis absorption and fluorescence emission spectra

UV/Vis spectra were recorded in a quartz cell (light path 10 mm) using a Shimadzu UV-3600 spectrophotometer equipped with a PTC-348WI temperature controller. Steady-state fluorescence spectra were recorded in a conventional quartz cell (light path 10 mm) using a Varian Cary Eclipse that was equipped using a Varian Cary single-cell Peltier accessory to control temperature.

DLS measurements

A sample solution (2 mL) was filtered through a 0.45 μm Millipore filter into a clean scintillation vial. The samples were examined using a laser-light scattering spectrometer (BI-200SM) equipped with a digital correlator (Turbo Correlator) at 636 nm at a scattering angle of $\theta = 90°$. For the determination of CAC by DLS measurements, the solvent was filtered through a 0.45 μm Millipore filter. The samples were dissolved in the filtered solvent and used without further filtering.

TEM measurements

A 5 μL portion of the dilute aqueous solution was dropped onto a copper grid. Then the grid was air-dried. The samples were examined using an FEI Tacnai 20 microscope operating at an accelerating voltage of 200 keV.

AFM measurements

A 25 μL portion of the dilute sample solution was dropped onto a new mica surface. Two minutes later, the excess amount of aqueous solution was blotted away with a piece of filter paper. The mica was washed with distilled water (1 mL) and then air-dried. The samples were examined using an AFM (Veeco Company, Multimode, Nano IIIa) in tapping mode in the air at room temperature.

SEM measurements

A 50 μL portion of the sample solution was dropped onto a coverslip followed by evaporating the liquid in air. The samples were examined using a Shimadzu SS-550 SEM operating at an accelerating voltage of 30 keV.

Preparation of 5-(4′-dodecyloxyphenyl)-10,15,20-tri(permethyl-β-CD)-modified Zn^{II}–porphyrin (1)

The synthesis of host **1** was carried out under typical click reaction conditions (Scheme 1). Firstly, the asymmertrical porphyrin was obtained according to a typical Adler method. 4-(Prop-2-ynyloxy)benzaldehyde (2.88 g, 18 mmol) and 4-dodecyloxybenzaldehyde (1.74 g, 6 mmol) were dissolved in propionic acid (500 mL) under rigorous stirring. After the resulting solution was heated to reflux, pyrrole (1.61 g, 24 mmol) was newly added and then the solution turned dark purple immediately. The solution was heated under reflux conditions for another 2 h, and propionic acid was then removed under reduced pressure. Triethylamine (10 mL) and methanol (400 mL) were added to the residue to precipitate the crude product. The precipitate was collected, washed with methanol

twice, and purified by means of column chromatography (dichloromethane/petroleum ether v/v 1:1) to give the final product.

The asymmetrical porphyrin **3** was obtained in 6% yield as a purple powder. ^{1}H NMR (400 MHz, CDCl$_3$): $\delta = 8.86$ (s, 8H), 8.14 (d, $J = 8.4$ Hz, 6H), 8.11 (d, $J = 8.4$ Hz, 2H), 7.37 (d, $J = 8.4$ Hz, 6H), 7.29 (s, 2H), 4.99 (d, $J = 2.1$ Hz, 6H), 4.25 (t, $J = 6.5$ Hz, 2H), 2.70 (t, $J = 1.9$ Hz, 3H), 2.01–1.96 (m, 2H), 1.64 (m, 2H), 1.30 (s, 18H), 0.88 (s, 3H), −2.77 ppm (s, 2H); ESI-MS: m/z: 961 $[M+H]^+$.

Zinc ions were introduced into the asymmetrical porphyrin **3** to avoid copper complexation in the next step. The asymmetrical porphyrin **3** was dissolved in chloroform/methanol (v/v 1:1) solution, then a 20-fold excess amount of zinc acetate in methanol was added. The solution was heated under reflux conditions for 5 h and then concentrated under reduced pressure. Chloroform (20 mL) was added in the residue and then filtrated to remove the unreacted zinc acetate. The filtrate was dried to obtain the final product 5-(4′-dodecyloxyphenyl)-10,15,20-tri(4′-propargyloxyphenyl)–Zn^{II}–porphyrin **3·Zn** in 100% yield. ESI-MS: m/z: 1023 $[M+H]^+$.

Compound **3·Zn** (102.4 mg, 0.1 mmol) and 6-deoxyl-6-azidopermethyl-β-CD (648 mg, 0.45 mmol) were dissolved in THF (20 mL) with stirring. CuSO$_4$·5H$_2$O (125 mg) and sodium ascorbate (150 mg) dissolved in water (20 mL) were added to the resulting solution. The mixture was heated at 60 °C for 48 h under an argon atmosphere and subsequently dried under reduced pressure. The obtained residue was dissolved in chloroform.

After insoluble precipitates were removed by filtration, the filtrate was dried and further purified by column chromatography (chloroform/methanol, v/v 30:1) to obtain product **1** as a violet powder in 90% yield. ^{1}H NMR (400 MHz, CDCl$_3$): $\delta = 8.95$ (s, 8H), 8.14 (d, $J = 8.2$ Hz, 6H), 8.10 (d, $J = 8.6$ Hz, 2H), 7.95 (s, 3H), 7.37 (d, $J = 8.2$ Hz, 6H), 7.29 (s, 2H), 5.48 (s, 6H), 5.34 (s, 3H), 5.23 (s, 3H), 5.15 (s, 15H), 4.85–4.76 (m, 3H), 4.24 (d, $J = 7.3$ Hz, 4H), 4.08–3.07 (m, 300H), 2.03–1.95 (m, 2H), 1.64 (m, 2H), 1.30 (s, 18H), 0.89 ppm (m, 3H); ^{13}C NMR (101 MHz, CDCl$_3$): $\delta = 158.1$, 150.6, 150.5, 150.4, 143.6, 135.9, 135.5, 131.8, 125.3, 112.8, 99.4, 99.3, 98.9, 98.8, 98.4, 83.1, 82.2, 82.1, 82.0, 81.9, 81.8, 81.2, 80.3, 80.2, 79.9, 79.4, 79.3, 71.5, 71.4, 71.0, 70.9, 70.8, 70.4, 62.4, 61.8, 61.5, 61.5, 61.3, 59.3, 59.2, 59.1, 59.0, 58.7, 58.6, 58.5, 58.4, 51.6, 32.0, 29.7, 29.6, 29.4, 26.3, 22.7, 14.2 ppm; MALDI-MS: m/z: 5368.4320 $[M+Na]^+$; elemental analysis calcd (%) for (C$_{251}$H$_{385}$N$_{13}$O$_{106}$Zn)(H$_2$O)$_6$: C 55.27, H 7.34, N 3.34; found: C 55.14, H 7.35, N 3.61.

Preparation of model compound 2

Model compound **2** was synthesized following a similar general procedure to that for the preparation of **1**. 5-(4′-Hydroxyphenyl)-10,15,20-tri(4′-propargyloxyphenyl)–porphyrin **4** was also synthesized by means of the Adler method and purified by column chromatography with dichloromethane as eluent in 5% yield. ^{1}H NMR (400 MHz, CDCl$_3$): $\delta = 8.87$ (s, 8H), 8.14 (d, $J = 8.5$ Hz, 6H), 8.08 (d, $J = 8.4$ Hz, 2H), 7.37 (d, $J = 8.5$ Hz, 6H), 7.20 (s, 2H), 4.99 (d, $J = 2.3$ Hz, 6H), 3.49 (s, 1H), 2.70 (t, $J = 2.3$ Hz, 3H), −2.78 ppm (s, 2H); ESI-MS: m/z: 792 $[M+H]^+$.

Zinc ions were also introduced into porphyrin **4** to obtain the product 5-(4′-hydroxyphenyl)-10,15,20-tri(4′-propargyloxyphenyl)–Zn^{II}–porphyrin **4·Zn** in 100% yield. ESI-MS: m/z: 855 $[M+H]^+$. Then, the reaction of **4·Zn** (85.6 mg, 0.1 mmol) and 6-deoxyl-6-azidopermethyl-β-CD (648 mg, 0.45 mmol) in the presence of CuSO$_4$·5H$_2$O (125 mg) and sodium ascorbate (150 mg) in THF/H$_2$O (v/v 1:1, 40 mL) was carried out under an argon atmosphere to afford product **2** in 70% yield. ^{1}H NMR (400 MHz, CDCl$_3$): $\delta = 9.02$–8.89 (m, 8H), 8.13 (d, $J = 8.2$ Hz, 6H), 8.07 (d, $J = 8.0$ Hz, 2H), 7.94 (d, $J = 5.1$ Hz, 3H), 7.36 (d, $J = 8.4$ Hz, 6H), 7.22 (d, $J = 8.0$ Hz, 2H), 5.46 (s,

6H), 5.33 (s, 3H), 5.22 (d, $J = 3.1$ Hz, 3H), 5.17–5.07 (m, 16H), 4.81 (dd, $J = 14.0$, 6.5 Hz, 3H), 4.22 (s, 3H), 4.08–3.09 ppm (m, 300H); ^{13}C NMR (101 MHz, CDCl$_3$): $\delta = 158.1$, 158.0, 150.5, 150.4, 143.6, 135.9, 135.5, 132.0, 131.9, 125.3, 120.5, 112.8, 100.0, 99.3, 98.9, 98.8, 98.4, 83.0, 82.1, 82.0, 81.8, 81.7, 81.2, 80.3, 80.2, 79.9, 79.4, 71.6, 71.4, 71.0, 70.8, 70.4, 62.3, 61.8, 61.5, 61.4, 61.3, 59.3, 59.2, 59.1, 59.0, 58.9, 58.7, 58.6, 58.5, 58.4, 51.5 ppm; MALDI-MS: m/z: 5200.2503 $[M+Na]^+$; elemental analysis calcd (%) for (C$_{239}$H$_{361}$N$_{13}$O$_{106}$Zn)(H$_2$O)$_6$: C 54.31, H 7.11, N 3.44; found: C 54.35, H 7.11, N 3.11.

Preparation of assemblies

Tetrasodium tetraphenylporphyrintetrasulfonate **5** was added to aqueous solutions of **1** (or **2**) in different molar ratios with stirring. Then the solutions were freeze-dried to obtain the final assemblies.

[1] a) R. Klajn, J. F. Stoddart, B. A. Grzybowski, *Chem. Soc. Rev.* **2010**, *39*, 2203–2237; b) H. Wang, K. Liu, K.-J. Chen, Y. Lu, S. Wang, W.-Y. Lin, F. Guo, K.-i. Kamei, Y.-C. Chen, M. Ohashi, M. Wang, M. A. Garcia, X.-Z. Zhao, C. K. F. Shen, H.-R. Tseng, *ACS Nano* **2010**, *4*, 6235–6243; c) X. Ma, H. Tian, *Acc. Chem. Res.* **2014**, *47*, 1971–1981; d) X. Yao, T. Li, S. Wang, X. Ma, H. Tian, *Chem. Commun.* **2014**, *50*, 7166–7168.

[2] a) Z. Tian, Y. Chen, W. Yang, J. Yao, L. Zhu, Z. Shuai, *Angew. Chem.* **2004**, *116*, 4152–4155; *Angew. Chem. Int. Ed.* **2004**, *43*, 4060–4063; b) H.-B. Fu, J.-N. Yao, *J. Am. Chem. Soc.* **2001**, *123*, 1434–1439; c) H. Fu, B. H. Loo, D. Xiao, R. Xie, X. Ji, J. Yao, B. Zhang, L. Zhang, *Angew. Chem.* **2002**, *114*, 1004–1007; *Angew. Chem. Int. Ed.* **2002**, *41*, 962–965; d) D. Xiao, L. Xi, W. Yang, H. Fu, Z. Shuai, Y. Fang, J. Yao, *J. Am. Chem. Soc.* **2003**, *125*, 6740–6745.

[3] a) A. O. Moughton, R. K. O'Reilly, *J. Am. Chem. Soc.* **2008**, *130*, 8714–8725; b) M. M. Conn, J. Rebek, *Chem. Rev.* **1997**, *97*, 1647–1668.

[4] G. M. Whitesides, B. Grzybowski, *Science* **2002**, *295*, 2418–2421.

[5] a) C.-H. Tung, L.-Z. Wu, L.-P. Zhang, B. Chen, *Acc. Chem. Res.* **2003**, *36*, 39–47; b) D.-S. Guo, K. Wang, Y.-X. Wang, Y. Liu, *J. Am. Chem. Soc.* **2012**, *134*, 10244–10250; c) K. Wang, D.-S. Guo, X. Wang, Y. Liu, *ACS Nano* **2011**, *5*, 2880–2894; d) S. K. M. Nalluri, J. Voskuhl, J. B. Bultema, E. J. Boekema, B. J. Ravoo, *Angew. Chem.* **2011**, *123*, 9921–9925; *Angew. Chem. Int. Ed.* **2011**, *50*, 9747–9751; e) M. Buaki, C. Aprile, A. Dhakshinamoorthy, M. Alvaro, H. Garcia, *Chem. Eur. J.* **2009**, *15*, 13082–13089; f) K. Kurihara, M. Tamura, K.-i. Shohda, T. Toyota, K. Suzuki, T. Sugawara, *Nat. Chem.* **2011**, *3*, 775–781; g) H. Jin, Y. Zheng, Y. Liu, H. Cheng, Y. Zhou, D. Yan, *Angew. Chem.* **2011**, *123*, 10536–10540; *Angew. Chem. Int. Ed.* **2011**, *50*, 10352–10356; h) Z. Nourian, W. Roelofsen, C. Danelon, *Angew. Chem.* **2012**, *124*, 3168–3172; *Angew. Chem. Int. Ed.* **2012**, *51*, 3114–3118.

[6] a) S. Virji, J. Huang, R. B. Kaner, B. H. Weiller, *Nano Lett.* **2004**, *4*, 491–496; b) A. La Torre, M. d. C. Giménez-López, M. W. Fay, G. A. Rance, W. A. Solomonsz, T. W. Chamberlain, P. D. Brown, A. N. Khlobystov, *ACS Nano* **2012**, *6*, 2000–2007; c) S. Tangbunsuk, G. R. Whittell, M. G. Ryadnov, G. W. M. Vandermeulen, D. N. Woolfson, I. Manners, *Chem. Eur. J.* **2012**, *18*, 2524–2535.

[7] a) D. Ke, C. Zhan, A. D. Q. Li, J. Yao, *Angew. Chem.* **2011**, *123*, 3799–3803; *Angew. Chem. Int. Ed.* **2011**, *50*, 3715–3719; b) A. Muñoz, B. M. Illescas, M. Sánchez-Navarro, J. Rojo, N. Martín, *J. Am. Chem. Soc.* **2011**, *133*, 16758–16761; c) C. Po, A. Y.-Y. Tam, K. M.-C. Wong, V. W.-W. Yam, *J.*

Am. Chem. Soc. **2011**, *133*, 12136–12143; d) M. R. Molla, S. Ghosh, *Chem. Eur. J.* **2012**, *18*, 9860–9869.

[8] a) Y. Li, X. Li, Y. Li, H. Liu, S. Wang, H. Gan, J. Li, N. Wang, X. He, D. Zhu, *Angew. Chem.* **2006**, *118*, 3721–3725; *Angew. Chem. Int. Ed.* **2006**, *45*, 3639–3643; b) Y. M. Zhang, Y. Chen, Y. Yang, P. Liu, Y. Liu, *Chem. Eur. J.* **2009**, *15*, 11333–11340; c) A. Mateo-Alonso, C. Ehli, G. M. Rahman, D. M. Guldi, G. Fioravanti, M. Marcaccio, F. Paolucci, M. Prato, *Angew. Chem.* **2007**, *119*, 3591–3595; *Angew. Chem. Int. Ed.* **2007**, *46*, 3521–3525; d) T. Haino, A. Watanabe, T. Hirao, T. Ikeda, *Angew. Chem.* **2012**, *124*, 1502–1505; *Angew. Chem. Int. Ed.* **2012**, *51*, 1473–1476; e) T. Haino, T. Fujii, A. Watanabe, U. Takayanagi, *Proc. Natl. Acad. Sci. USA* **2009**, *106*, 10477–10481; f) F. J. M. Hoeben, M. Wolffs, J. Zhang, S. De Feyter, P. Leclère, A. P. H. J. Schenning, E. W. Meijer, *J. Am. Chem. Soc.* **2007**, *129*, 9819–9828.

[9] a) Y. Liu, C.-F. Ke, H.-Y. Zhang, J. Cui, F. Ding, *J. Am. Chem. Soc.* **2008**, *130*, 600–605; b) M. Fathalla, A. Neuberger, S.-C. Li, R. Schmehl, U. Diebold, J. Jayawickramarajah, *J. Am. Chem. Soc.* **2010**, *132*, 9966–9967; c) N. Kandoth, E. Vittorino, M. T. Sciortino, T. Parisi, I. Colao, A. Mazzaglia, S. Sortino, *Chem. Eur. J.* **2012**, *18*, 1684–1690; d) M. Bonchio, T. Carofiglio, M. Carraro, R. Fornasier, U. Tonellato, *Org. Lett.* **2002**, *4*, 4635–4637; e) A. Mulder, A. Juković, F. W. B. van Leeuwen, H. Kooijman, A. L. Spek, J. Huskens, D. N. Reinhoudt, *Chem. Eur. J.* **2004**, *10*, 1114–1123; f) L. Li, H.-Y. Zhang, J. Zhao, Y. Liu, *Chem. J. Chin. Univ.* **2013**, *34*, 1640–1645.

[10] a) Z.-Y. Gu, D.-S. Guo, M. Sun, Y. Liu, *J. Org. Chem.* **2010**, *75*, 3600–3607; b) J. Králová, Z. k. Kejík, T. s. Bříza, P. Poučková, A. Král, P. Martásek, V. Král, *J. Med. Chem.* **2010**, *53*, 128–138; c) F. Quaglia, L. Ostacolo, A. Mazzaglia, V. Villari, D. Zaccaria, M. T. Sciortino, *Biomaterials* **2009**, *30*, 374–382; d) A. Mazzaglia, N. Angelini, R. Darcy, R. Donohue, D. Lombardo, N. Micali, M. T. Sciortino, V. Villari, L. M. Scolaro, *Chem. Eur. J.* **2003**, *9*, 5762–5769; e) K. Kano, H. Kitagishi, M. Kodera, S. Hirota, *Angew. Chem.* **2005**, *117*, 439–442; *Angew. Chem. Int. Ed.* **2005**, *44*, 435–438; f) H. Kitagishi, S. Negi, A. Kiriyama, A. Honbo, Y. Sugiura, A. T. Kawaguchi, K. Kano, *Angew. Chem.* **2010**, *122*, 1334–1337; *Angew. Chem. Int. Ed.* **2010**, *49*, 1312–1315; g) K. Kano, H. Kitagishi, S. Tamura, A. Yamada, *J. Am. Chem. Soc.* **2004**, *126*, 15202–15210; h) R. Breslow, X. Zhang, R. Xu, M. Maletic, R. Merger, *J. Am. Chem. Soc.* **1996**, *118*, 11678–11679; i) J. Yang, B. Gabriele, S. Belvedere, Y. Huang, R. Breslow, *J. Org. Chem.* **2002**, *67*, 5057–5067.

[11] D. Adler, F. R. Longo, W. Shergalis, *J. Am. Chem. Soc.* **1964**, *86*, 3145–3149.

[12] a) W. Tao, Y. Liu, B. Jiang, S. Yu, W. Huang, Y. Zhou, D. Yan, *J. Am. Chem. Soc.* **2012**, *134*, 762–764; b) J. Zou, B. Guan, X. Liao, M. Jiang, F. Tao, *Macromolecules* **2009**, *42*, 7465–7473.

[13] T. Haino, Y. Matsumoto, Y. Fukazawa, *J. Am. Chem. Soc.* **2005**, *127*, 8936–8937.

[14] The ζ potential of the vesicular assembly was measured to be −30.20 mV, whereas it increased to −55.33 mV after the addition of an excess amount of **5**. These observations further indicate the embedding phenomenon of an excess amount of **5** in the vesicles (Figures S40–S42 in the Supporting Information).

[15] As for complex **1·5** in a 1:1.0 stoichiometric ratio, the morphologies of the assembly were also investigated by TEM images. Firstly, the vesicular assemblies can be observed from the sample prepared by using an aqueous solution of the fresh complex **1·5**. After the solution of complex **1·5** remained for several hours, the vesicular aggregates disappeared and formed some amorphous aggregations.

[16] a) S. Houmadi, D. Coquière, L. Legrand, M. C. Fauré, M. Goldmann, O. Reinaud, S. Rémita, *Langmuir* **2007**, *23*, 4849–4855; b) P. Quagliotto, N. Barbero, C. Barolo, K. Costabello, L. Marchese, S. Coluccia, K. Kalyanasundaram, G. Viscardi, *Dyes Pigm.* **2009**, *82*, 124–129.

[17] a) R. Nishiyabu, K. Kano, *Eur. J. Org. Chem.* **2004**, 4985–4988; b) K. Yamauchi, A. Miyawaki, Y. Takashima, H. Yamaguchi, A. Harada, *Org. Lett.* **2010**, *12*, 1284–1286; c) S. Menuel, N. Azaroual, D. Landy, N. Six, F. Hapiot, E. Monflier, *Chem. Eur. J.* **2011**, *17*, 3949–3955.

[18] The peaks of the protons of **5** were broadened in D_2O owing to self-aggregation of **5** in aqueous solution. To solve this problem, tetrasodium-*meso*-tetra(4-sulfonatophenyl)zinc(II) porphyrin **Zn·5** was used for NMR spectroscopic studies.

[19] a) J. Li, L. Zhou, Q. Luo, Y. Wang, C. Zhang, W. Lu, J. Xu, J. Liu, *Chin. J. Chem.* **2012**, *30*, 2085–2090; b) M. Popov, S. Grinberg, C. Linder, T. Waner, B. Levi-Hevroni, R. J. Deckelbaum, E. Heldman, *J. Controlled Release* **2012**, *160*, 306–314; c) H. Kuang, S. Wu, Z. Xie, F. Meng, X. Jing, Y. Huang, *Biomacromolecules* **2012**, *13*, 3004–3012.